

We are IntechOpen, the world's leading publisher of Open Access books Built by scientists, for scientists

6,900

Open access books available

185,000

International authors and editors

200M

Downloads

Our authors are among the

154

Countries delivered to

TOP 1%

most cited scientists

12.2%

Contributors from top 500 universities



WEB OF SCIENCE™

Selection of our books indexed in the Book Citation Index
in Web of Science™ Core Collection (BKCI)

Interested in publishing with us?
Contact book.department@intechopen.com

Numbers displayed above are based on latest data collected.
For more information visit www.intechopen.com



Paramagnetic Transitions Ions as Structural Modifiers in Ferroelectrics

Veronica Lucero Villegas Rueda

Abstract

The science of ferroelectric materials has long known that transition metal atom and/or rare earth atom substitution in the composition of a ferroelectric material can produce substantial structural and electric dipole changes and ferroelectric behavior. The focus is on first neighbor changes, symmetry, very tiny atomic displacements, hence magnitudes of electric polarization, charge changes, and mechanical-tensile change of parameters. The transition atom used for the substitution can, or, cannot be paramagnetic. When it is paramagnetic as is the case with Cr^{3+} , Mn^{2+} and so forth, there emerges an advantage for its experimental characterization at atomic level. Electron Paramagnetic Resonance (EPR) allows the identification of its location within the structure and the number and nature of its neighbors. The presence of crystal fields, symmetry and distortions of the first coordination sphere can also be determined. Here, we describe how a set of EPR spectra is analyzed to extract such atomic information.

Keywords: paramagnetic transition ions, ferroelectrics, $PbTiO$ (Cr), octahedral symmetry, electron paramagnetic resonance, crystal field

1. Introduction

The ferroelectric materials are very important for technological applications in general, like sensor and actuators they are important part of electronic devices. The temperature, pressure, electric and electromagnetic field nonlinear response of ferroelectrics make them ideal like active elements due to pyroelectric and piezoelectric effects [1–4]. Ferroelectrics are used like ultrasonic generator; high voltage transformers and accelerators [1–4], also, they are using in optical components, piezoelectric transducers, and pyroelectric sensors [1–4]. By fabrication ferroelectric materials born with electric dipole different to zero, $P \neq 0$; this electric property is by asymmetry crystalline center structure. The **Figure 1** shows two crystalline structures, first is a symmetry perovskite structure with $P = 0$, and second is an asymmetry perovskite structure with $P \neq 0$ typical to lead titanate ($PbTiO_3$) [5]. The lead titanate ($PbTiO_3$) is used intensively in electronic devices [5–7]. The $PbTiO_3$ ceramic had perovskite structure (tetragonal structure) with ratio $c/a = 1.064$, where $c = 4.154\text{\AA}$, $a = 3.899\text{\AA}$, the **Figure 1a** shows the lead ion (Pb) occupies places A, the titanium ion (Ti) occupies the places B and the oxygen ion is on the parallelepiped faces occupies the places O [8].

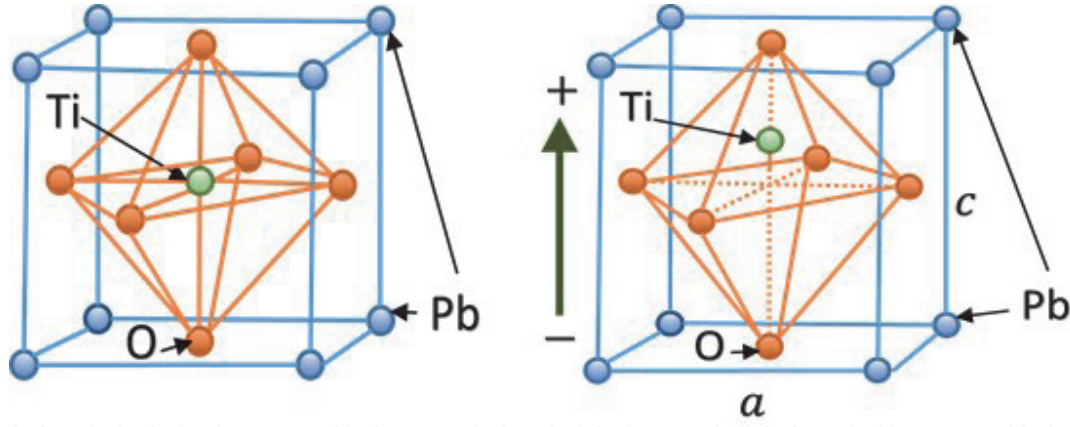


Figure 1.

The perovskite structure for PbTiO_3 a) Centre symmetry and b) non Centre with ratio $c/a = 1.064$, where $c = 4.154\text{\AA}$, $a = 3.899\text{\AA}$.

The ceramic fragility is reduced for inserting rare earths or transition metal atoms [6–8]. The partial or total substitution of Pb or Ti produces modified compounds with new electrical polarization and modifies their structure depending on doping atoms and the interactions material [8]. The changes in the structure could be small or big depending on the kind of dopant and the percentage of them [1–8]. If the dopant is a paramagnetic ion, it could be detected by paramagnetic resonance (EPR) and it is capable to sense structure changes principally by spin-orbit interactions [9–11].

The paramagnetic resonance technique (EPR) detects the spin-orbital magnetic interaction in doped ferroelectrics when the dopant is a rare earth with a paramagnetic ion. If the dopant is chromium (Cr), it can give a paramagnetic state; in this case, the electron paramagnetic resonance (EPR) technique is capable to detect paramagnetic ions, and the EPR-technique is highly sensitive to spin interactions due to crystalline structure, nuclear interaction (hyperfine), or anisotropies (orientations) [9–11]. The nondestructive EPR-technique is applied to organic and inorganic molecules, ions, and atoms that have unpaired electrons that have information about oxidation state and spin state due to unpaired electron spin [9–11]. The EPR technique uses microwave energy to induce resonances or electron transitions between electronic energy levels separated by applying a magnetic field for paramagnetic compounds or substances. The typical EPR spectra for Cr, Fe, Mn, Co, Ni, Cu, V, etc. [11–15] contained information about the g -factor, the A -hyperfine couple, and crystalline field factors, D and E .

2. Atoms into magnetic field \vec{H}

The energy interaction between magnetic moment $\vec{\mu}$ and external magnetic field \vec{H} is given by $W = -\vec{\mu} \cdot \vec{H}$. The electronic orbital movement is the cause of atomic momentum for the atom $\vec{\mu}$; it is proportional to angular momentum \vec{L} given by $\vec{\mu}_L = \left(-\frac{e}{2mc}\right)\vec{L}$, where \vec{L} is the orbital angular momentum, e is the electron charge, m is the electron mass, and c is the speed of light. The gyromagnetic ratio is defined by $\gamma \equiv \frac{e}{2mc} = 1.7 \times 10^7 \text{ rad gauss}^{-1}$, so the atomic momentum is given by $\vec{\mu}_L = \gamma \vec{L}$ [9].

Otherwise, the intrinsic magnetic moment for electron is $\vec{\mu}_S = 2\left(-\frac{e}{2mc}\right)\vec{S}$, where \vec{S} is the spin vector associated to electron spin. The total magnetic moment is given by the spin and orbital momentum addition $\vec{\mu} = \vec{\mu}_L + \vec{\mu}_S$. If the total magnetic moment is placed into magnetic field \vec{H} , the total magnetic energy is given

by $W = -\vec{\mu} \cdot \vec{H} = -\mu H \cos \theta$, where θ is the angle between vectors $\vec{\mu}$ and \vec{H} , the angle could varies continually in the classical description, however, in the quantum mechanics description the variation is quantized with $2J + 1$ orientations, where J is the quantum number for the total angular momentum given by $\sqrt{J(J+1)}\hbar$ [9, 12]. The allowed projections J , when the system is quantized along the magnetic field direction, are given by $m_j\hbar$, where m_j is the quantum magnetic number with values from $J, J - 1, \dots, -J$ [15].

The simplest case is just only the spin electronic momentum (atoms in base state $^2S_{1/2}$) with $m_S = S, S - 1, \dots, -S$, with S the total electronic spin, and the projections are $|\vec{\mu}_S| = 2(-\frac{eh}{4\pi mc})m_S$ where for \vec{S} operator the eigenvalue $m_S\hbar$ was substituted. The quantity $\frac{eh}{4\pi mc} \equiv \beta_e = 9.2741 \times 10^{-21} \text{ erg/gauss}$ is called Bohr's magneton, then $|\vec{\mu}_S| = \beta_e m_S$ and the energy values allowed for the atom placed into a magnetic field \vec{H} , are $E_{m_S} = -\mu_S H = 2\beta_e m_S H$ (Zeeman's energy). For an electron isolate quantum electrodynamic correction is necessary [9–15] replacing the number 2 for the $g_e = 2.00023$. In the case for isolate spin $S = 1/2$, the $2S + 1$ energy levels are $g_e\beta_e H$ equally spaced, the **Figure 2** shows the case for $S = 1/2$ [9–15].

For degenerated orbital state ($L \neq 0$) where exist and important L and S coupling (Russell-Saunders coupled) [9–15] there are $J = L + S, L + S - 1, \dots, |L - S|$, and for each J there are $m_J = J, J - 1, \dots, -J$ values, so the energy for each degenerated state is $E_{m_J} = g_J\beta_e m_J H$, where $g_J = 1 + \frac{J(J+1)+S(S+1)-L(L+1)}{2J(J+1)}$ is the splitting Landé factor. For example, the state $^2P_{1/2}$ have $S = 1/2, L = 1, J = 1/2$ and then $g = 3/2$. Of course, when $L = 0$ the $g_J = g_e$ [9].

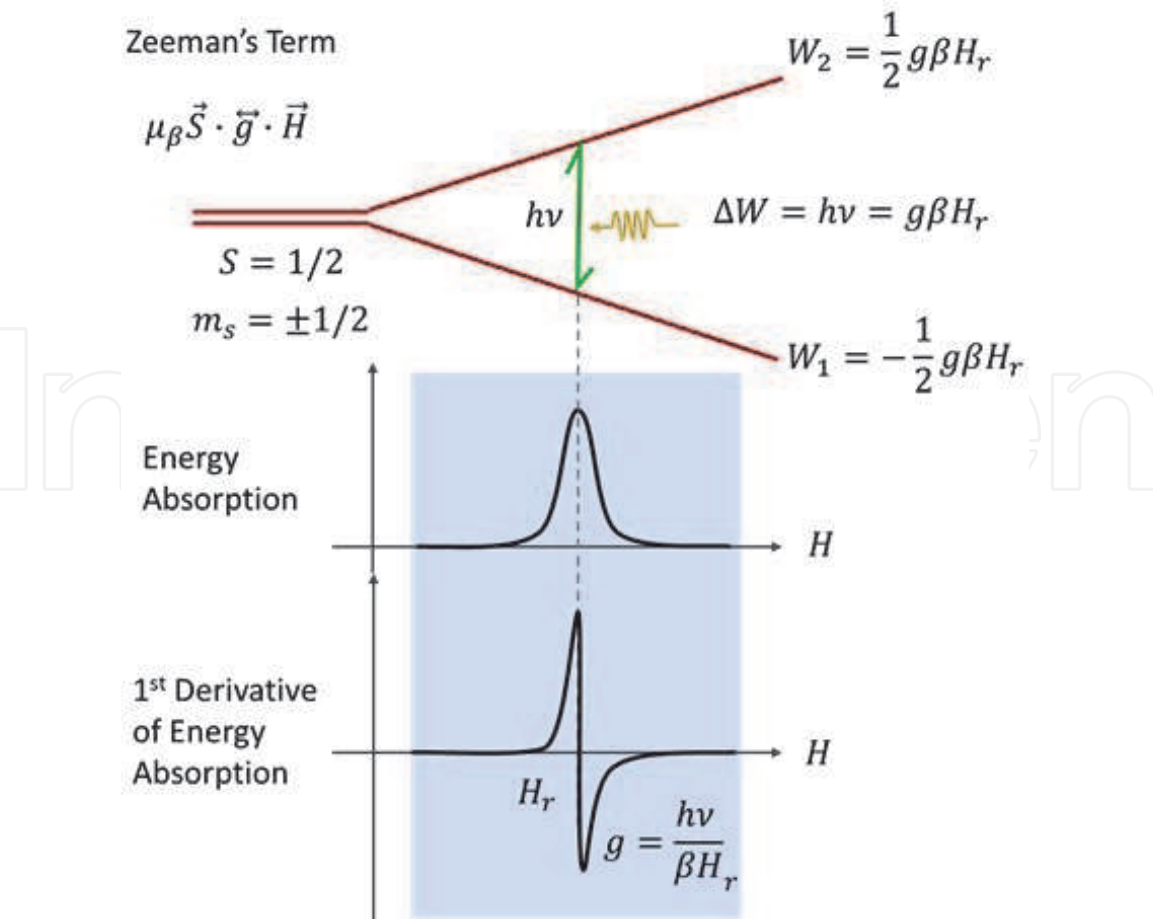


Figure 2. EPR scheme for system with $S = 1/2$. The Zeeman's effect for $S = 1/2$ split the degenerate state energy into W_1 and W_2 and the microwave photon $h\nu$ provide the energy for the transition between them [14].

3. The basic principle of the electron paramagnetic resonance (EPR) spectroscopy

The splitting of the degenerate energy levels applying magnetic field is the principle of the paramagnetic resonance spectroscopy useful for study the paramagnetic materials with total electronic spin $\vec{S} \neq 0$. The splitting of the electronic energy levels occurs when a magnetic field \vec{H} is applied, this phenomenon is called Zeeman's effect. In the experiment an oscillating microwave field is applied to give energy to the electrons so the electronic transition of the electrons can occur; these electrons are arranged in the electronic levels according to Hund's rule. From quantum mechanics point of view, when the microwave energy photon $h\nu$ is equal to the energy difference between Zeeman levels there are electrons transitions from one low electronic energy level (W_1) to other with high energy (W_2); the energy difference between this electronic energy levels is $\Delta W = W_2 - W_1 = h\nu$, according to quantum mechanics selection rules [10, 12]. When $\Delta W = h\nu$ occurs, there are peaks of microwave energy absorptions observed in the EPR spectrum. Experimentally a high resolution for the EPR spectrum is obtained taken the first derivative of absorption [9–15].

In general, the splitting electronic levels effect is written tensorial form by $\mu_B \vec{S} \cdot \vec{g} \cdot \vec{H}$. The photon energy $h\nu$ of the microwaves is provided to the system applying an oscillating microwave electromagnetic field \vec{H}_1 at frequency ν_0 ; the $\vec{H}_1(t)$ is applied perpendicularly to \vec{H}_0 magnetic field, and the magnitude of H_0 is varied until the resonance condition given in Eq. (1) be satisfied.

$$h\nu = g\beta H \quad (1)$$

For the simplest case for “free ion” and spin $S = 1/2$ system the Eq. (1) is reduced to $\Delta W = h\nu_0 = g_e \beta_e H_0$, where g_e is the gyromagnetic ratio and β_e is the Bohr's magneton for free electron e ; the EPR scheme is shown in **Figure 2**. The constants value $g_e = 2.0023$ and $\beta_e = 9.2741 \times 10^{-21} \text{ erg/gauss}$, the Planck's constant is $h = 6.6262 \times 10^{-27} \text{ ergs}$ [9, 15]. In general, these energy levels are described by tensorial treatment.

4. Spin Hamiltonian

For a paramagnetic ion, the energy levels are quantized. This energy levels are eigenvalues of the spin Hamiltonian operator which is the representation of total electronic energy for the ion or system. Usually the lowest energy levels states are populated at ordinary temperatures of $300K$ ($\approx 200 \text{ cm}^{-1}$) and this is the group of levels of the ground state. The ground state is the most of the times the only involved in the resonance experiment, it is to say, the transition are induced between this energy levels of ground state under microwave excitation. The energy of each level depends of the ion properties like electric charge, mass, atomic number, etc. and the energy level depends too to the crystalline field effect and the external magnetic field applied along with appropriate nuclear interactions [9, 12, 15].

The EPR results are interpreted by spin Hamiltonian that describes the system and the interactions mentioned above. The Hamiltonian is given in general by Eq. (2) and Eq. (3) [9–12].

$$\hat{H} = \beta \vec{S} \cdot \vec{g} \cdot \vec{H} + \vec{S} \cdot \vec{A} \cdot \vec{I} + \vec{S} \cdot \vec{D} \cdot \vec{S} \quad (2)$$

$$\hat{H} = g\beta \vec{S} \cdot \vec{H} + A\vec{S} \cdot \vec{I} + D \left[S_x^2 - \frac{1}{3}S(S+1) \right] + E(S_x^2 - S_y^2) \quad (3)$$

The first term is by Zeeman electronic interaction, the second term is the representation of hyperfine interaction, the third and fourth terms are due to the crystalline field, where \vec{g} , \vec{A} and \vec{D} are the spectroscopy, hyperfine interaction and crystalline field third order tensors respectively.

The magnetic interaction is naturally anisotropic, and the tensors are used to describe it, like the magnetic moment for each electron $\vec{\mu}$. The anisotropy property for magnetic moment $\vec{\mu}$ is measured by spectroscopy factor \vec{g} .

The solutions for the Hamiltonian are compared with measures of g parameters in the spectrum EPR and other paramagnetic parameters in the system [9–12].

4.1 Zeeman electronic term

The general expression for Zeeman interaction between external magnetic field \vec{H}_0 and the electronic spin \vec{S} is given in Eq. (4) and it is rewritten in terms of matrix in Eq. (5) [9–15].

$$\hat{H}_{Ze} = \beta \vec{S} \cdot \vec{g} \cdot \vec{H}_0 \quad (4)$$

$$\hat{H}_{Ze} = \beta \begin{pmatrix} S_x & S_y & S_z \end{pmatrix} \begin{pmatrix} g_{xx} & g_{xy} & g_{xz} \\ g_{yx} & g_{yy} & g_{yz} \\ g_{zx} & g_{zy} & g_{zz} \end{pmatrix} \begin{pmatrix} H_x \\ H_y \\ H_z \end{pmatrix} \quad (5)$$

Where $H_x, H_y, H_z, S_x, S_y, S_z$, are the three scalar components for external magnetic field \vec{H}_0 and \vec{S} in a fixed Cartesian coordinates x, y and z in the molecule.

Many times is found that tensor \vec{g} is a symmetric matrix, which could be diagonalized through appropriate transformation [9, 16] $M\vec{g}M^{-1} = \vec{g}_{diagonal}$. This transformation corresponds to axes reorientation and the matrix M redefine the orientation for new principal axes respecting to previous axes. After to diagonalized the Zeeman's Hamiltonian writes like Eq. (6).

$$\hat{H}_{Ze} = \beta (g_{xx}H_xS_x + g_{yy}H_yS_y + g_{zz}H_zS_z) \quad (6)$$

The \vec{g} components g_{xx}, g_{yy} and g_{zz} measured the contribution of magnetic moment along principal direction xx, yy and zz of magnetic field. There is spherical symmetry for the electron $\vec{\mu}(g)$ when $g_{xx} = g_{yy} = g_{zz}$.

The Hydrogen atom have spherical symmetry, the spin Hamiltonian have a g isotropic factor for an electron and isotropic hyperfine interaction, A , between electron and nucleus. In the most molecules these quantities vary with applied magnetic field direction and the spin Hamiltonian is anisotropic [9–16].

4.2 Axial symmetry

If the \vec{g} tensor is anisotropic, there is the axial symmetry when $g_{xx} = g_{yy} \neq g_{zz}$. Usually the EPR bibliography writes $g_{xx} = g_{yy} = g_{\perp}$ and $g_{zz} = g_{\parallel}$ [9–12].

Suppose that magnetic field \vec{H} is applied with θ angle respect to z -axis. Rewriting the components, $H \cos \theta$ is parallel to z and $H \sin \theta$ is parallel to x , then the Zeeman \hat{H}_{Ze} writes like Eq. (7) [9].

$$\hat{H}_{Ze} = \beta H (g_{\parallel} S_z \cos \theta + g_{\perp} S_x \sin \theta) \quad (7)$$

Where $S_x = \frac{1}{2}(S_+ + S_-)$ written in terms of created and annihilated spin operators. With low symmetry and magnetic field random oriented, using the director cosines l, m, n with respect x, y and z axis, then the spin Hamiltonian writes like Eq. (8).

$$\hat{H}_{Ze} = \beta H (g_{xx} l S_x + g_{yy} m S_y + g_{zz} n S_z) \quad (8)$$

This correspond to rhombic symmetry $g_{xx} \neq g_{yy} \neq g_{zz}$.

For the axial asymmetry g factor is dependent of angle θ by $g(\theta)^2 = g_{\perp}^2 \sin^2 \theta + g_{\parallel}^2 \cos^2 \theta$, for an axial g matrix with $g_{\parallel} > g_{\perp}$, the line shape of the corresponding EPR spectrum are drawn in **Figure 3**, assuming a large number of paramagnetic systems with random orientation of their \vec{g} ellipsoids with respect to the static magnetic field \vec{H} [9]. This situation is typical for a powder sample that contain all possible direction g -ellipsoids. For a given magnetic strength H , all spins fulfilling the resonance condition $g(\theta) = h\nu/\beta H$, i. e., all spins for which H makes an angle θ with the z -axis of the g -ellipsoid, contribute to the spectrum and are considered to form a spin packet. The extreme positions ($\theta = 0^\circ$ and $\theta = 90^\circ$) of the powder spectrum are obtained by inserting g_{\parallel} and g_{\perp} into the resonance condition. If $g_{\parallel} > g_{\perp}$ the asymmetry line shape is mainly due to the fact that the number of the spin packets contributing to the spectrum is much larger in the xy -plane than the along the z -axis. If $g_{\parallel} < g_{\perp}$ the asymmetry line shape is mainly due to the fact that the number of the spin packets contributing to the spectrum is much larger along the z -axis than in the xy -plane. Also, by definition the $g_{iso} = \sqrt{\frac{1}{3} [g_{xx}^2 + g_{yy}^2 + g_{zz}^2]}$ [9–17].

4.3 Hyperfine interaction term

The hyperfine interaction is the interaction between decoupled electrons (\vec{S}) and nuclear magnetic moments (\vec{I}) of several neighboring nucleus. In the EPR spectra the hyperfine split is due to interaction between electronic spin and nuclear spin, it causes splitting Zeeman levels. Each Zeeman level is splitting $2I + 1$ times, where I is the nuclear spin [12, 16]. In tensorial form the Hamiltonian spin term is given by $\vec{S} \cdot \vec{A} \cdot \vec{I}$. Similarly to g -factor, the A -hyperfine factor give the magnitude of hyperfine interaction, in general it is an anisotropic tensor. There are two types of hyperfine interaction [9–15].

The first interaction is the classic interaction between $\vec{\mu}_S$ and $\vec{\mu}_I$ dipoles separated a \vec{r} distance given by Eq. (9) [9, 12].

$$E_{dip} = \frac{\vec{\mu}_S \cdot \vec{\mu}_I}{r^3} - \frac{3(\vec{\mu}_S \cdot \vec{r})(\vec{\mu}_I \cdot \vec{r})}{r^5} \quad (9)$$

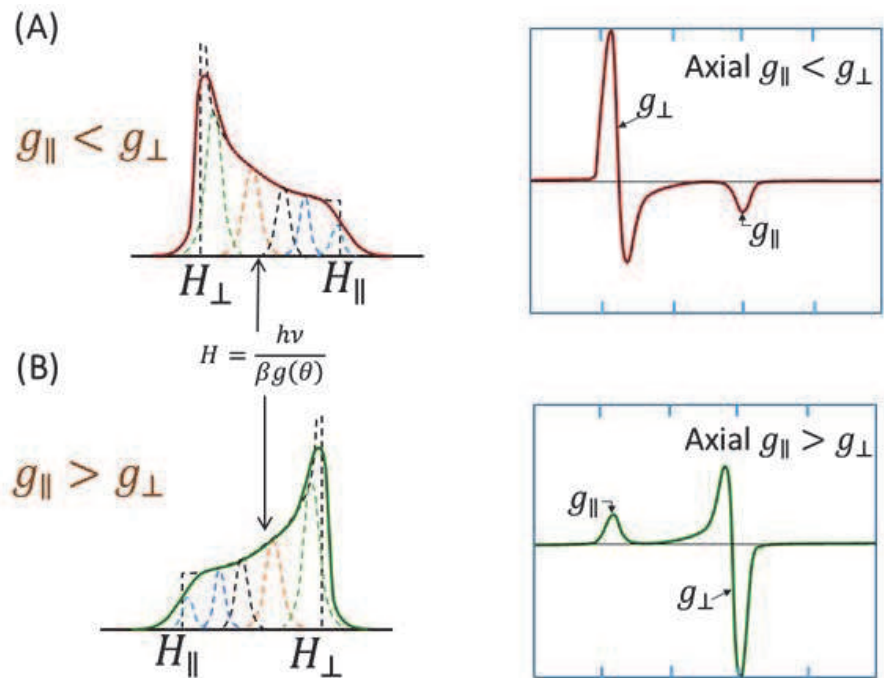


Figure 3. Microwave absorption spectra and their first derivate for axial symmetry (A) $g_{\parallel} > g_{\perp}$ and (B) $g_{\parallel} < g_{\perp}$. Both cases show all contributions for all directions contributions of $g(\theta) = h\nu/\beta H$ in a powder samples [9–16].

For correspondence principle, the quantum Hamiltonian for this interaction is given in Eq. (10).

$$\hat{H}_{dip} = g_e \beta_e g_n \beta_n \left[\frac{\vec{S} \cdot \vec{I}}{r^3} + \frac{3(\vec{I} \cdot \vec{r})(\vec{S} \cdot \vec{r})}{r^5} \right] \quad (10)$$

The second interaction is no classic interaction and comes from to the probability different of zero for found an electron in the nuclear region ($0 < r < a_0$), where a_0 is the Bohr's radii, i.e., it is proportional to the square electronic function valuated in the nucleus. Fermi proof that this interaction is isotropy and is called contact interaction or Fermi's interactions, given by Eq. (11) [10–17]. Here $\Psi(0)$ is the electronic wave function valued in the nucleus.

$$\hat{H} = \left(\frac{8\pi}{3} \right) \vec{\mu}_S \cdot \vec{\mu}_n |\Psi(0)|^2 \quad (11)$$

If the molecule have one or more neighboring nuclei to the uncoupled magnetic dipolar momentum, it turns out split hyperfine of energy magnetic levels of the decoupled electron (even without external magnetic field applied) due to interaction of each nucleus with the electronic magnetic momentum.

When the conditions are favorable the hyperfine interaction could be measured like in the case of the hyperfine interaction splitting of an octahedral manganese(II) complex with spin $S = 5/2$ and nuclear spin $I = 5/2$ and the corresponding EPR spectrum are shown in the Drago's book at Figure 13.10 [9].

In the simplest case, the energy levels of a system with one unpaired electron and one nucleus with $I = 1/2$ are show in **Figure 4(A)** with sufficiently high fixed magnetic field \vec{H} . The dashed line would be the transition corresponding to $\Delta W = h\nu = g\beta H$ in the absence of hyperfine (A_0), like is show in **Figure 2**. The solid lines

marked ΔW_1 and ΔW_2 correspond to the allowed EPR transitions with the hyperfine coupling operative. To first order, $h\nu = g\beta H \pm \frac{1}{2}A_0$, where A_0 is the isotropic hyperfine coupling constant. In **Figure 4(B)** are shown the hyperfine splitting as a function of an applied magnetic field. The dashed line corresponds to the transitions in the case of $A_0 = 0$. The solid lines ΔW_1 and ΔW_2 refer to transitions induced by a constant microwave quantum $h\nu$ of the same energy as for the transition ΔW . Here the resonant-field values corresponding to these two transitions are, to first order, given by $H = h\nu/g\beta \pm 1/2(g_e/g)a_0$ (in mT) is the hyperfine splitting constant given approximately by $H_{\Delta W_1} - H_{\Delta W_2}$. Note that these diagrams are specific to a nucleus with positive g_n and A_0 values, such as hydrogen atom [9, 12]. The **Figure 4(C)** shows the typical EPR spectrum and the g - value approximate positions for the case described in (A) and (B) with a_0 hyperfine splitting, and additionally shows the hyperfine splitting for and axial symmetry EPR signal with A_{\parallel} and A_{\perp} splitting factor than indicating how hyperfine interactions is affecting the energy levels transitions [11, 12].

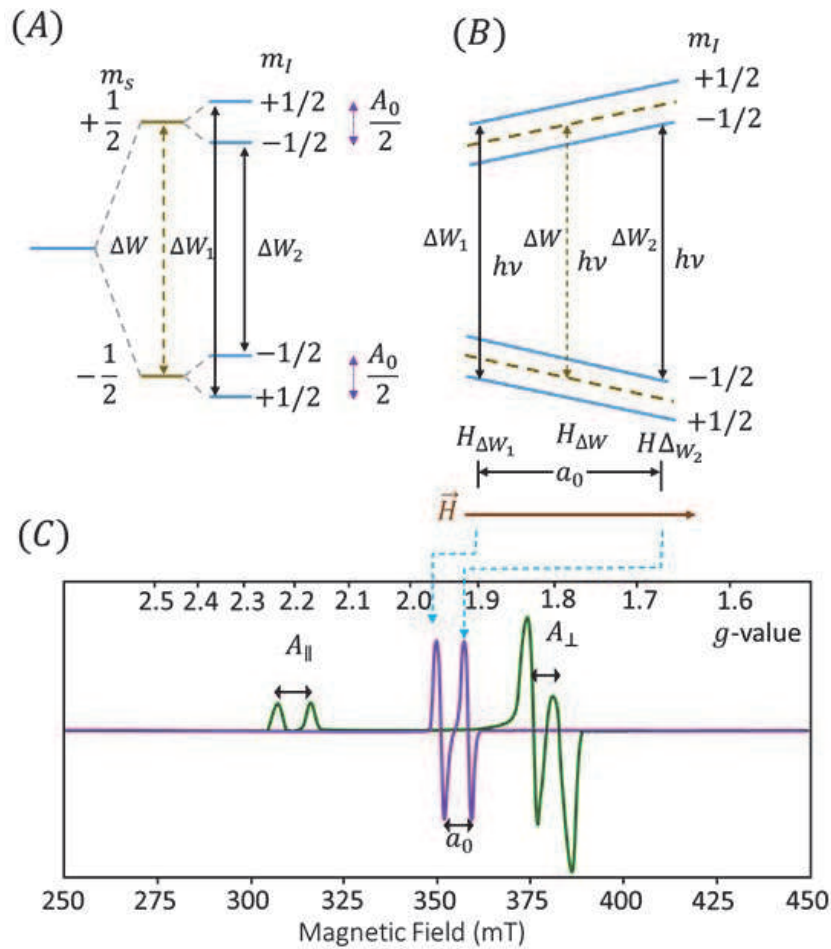


Figure 4.

(A) At a sufficiently high fixed magnetic field \vec{H} . The dashed line would be the transition corresponding to $\Delta W = h\nu = g\beta H$ in the absence of hyperfine (A_0). The solid lines marked ΔW_1 and ΔW_2 correspond to the allowed EPR transitions with the hyperfine coupling operative. To first order, $\Delta W = h\nu = g\beta H \pm \frac{1}{2}A_0$, where A_0 is the isotropic hyperfine coupling constant. (B) As a function of an applied magnetic field. The dashed line corresponds to the transitions in the hypothetical case of $A_0 = 0$. The solid lines ΔW_1 and ΔW_2 refer to transitions induced by a constant microwave quantum $h\nu$ of the same energy as for the transition ΔW . Here the resonant-field values corresponding to these two transitions are, to first order, given by $H = h\nu/g\beta \pm 1/2(g_e/g)a_0$ (in mT) is the hyperfine splitting constant. (C) Shows the typical EPR spectrum and the g - value approximate positions for the case described in (A) and (B) with a_0 hyperfine splitting, and additionally shows the hyperfine splitting for and axial symmetry EPR signal with A_{\parallel} and A_{\perp} splitting factor than indicating how hyperfine interactions is affecting the energy levels transitions [11, 12].

4.4 Crystalline field term

Other observable interaction in EPR is the crystalline field [9–17], this interaction is represented by tensors given by $\vec{S} \cdot \vec{D} \cdot \vec{S}$. This is the interaction of electron spin with the electric field of the charges of the neighboring ions placed in specific symmetries. The expression for crystalline field is given by [9–12]:

$$D \left[S_x^2 - \frac{1}{3} S(S+1) \right] + E (S_x^2 - S_y^2) \tag{12}$$

The Zero-field splitting parameters D and E split the energies of m_s levels at zero applied magnetic field according to the magnitude of m_s for each level. Thus the D and E ensure the singularity of each energy gap between m_s levels under a non-zero magnetic field. The magnitudes of D and E are dependent on the ligand field theory (or from the Crystal Field Theory point view), and therefore are easily tunable by coordination geometry [12, 18]. Even the g – factor could give in terms of crystal splitting factor Δ [11, 12, 18].

The **Figure 5** shows how the splitting of electronic levels depends on the ion interaction with electric field of the neighboring charge ions placed in specific symmetries [9–12].

The crystal field splitting energy Δ is the energy of repulsion between electrons of the ligands and the central metal ion and their bounding in complex ions such as octahedral, square planar and tetrahedral structural symmetries [9, 12]. If the Δ is greater than electron spin pairing energy the greater stability would be obtained if the fourth and fifth electrons get paired with the ones in lower level. If the Δ is less than the pairing energy, greater stability is obtained by keeping the electrons unpaired. So, if Δ is weak then the spin S is high and this yields a strongly

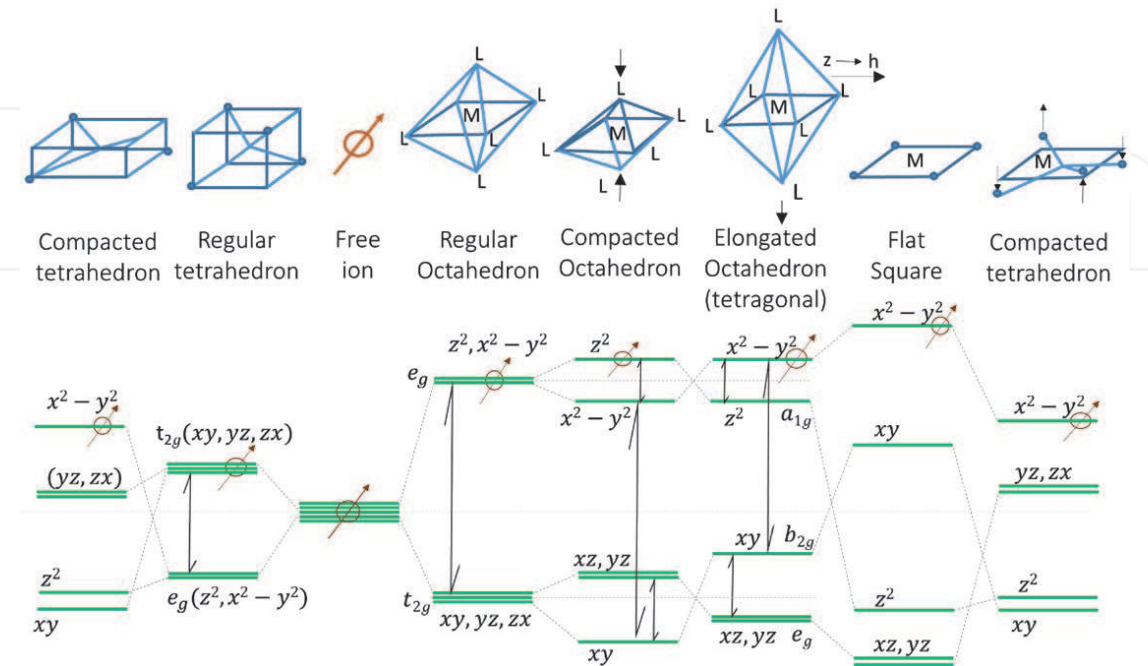


Figure 5. Crystalline field interaction for a 3d electron with neighboring placed in specific symmetries, below are the corresponding splits electronic levels. The splitting levels have crystal field splitting energy Δ or in terms of D and E zero-field splitting parameters [9–17].

paramagnetic complexes, and if Δ is high then the spin S is weak and this yields low spin complexes and weakly paramagnetic or sometimes even diamagnetic. Through microwave excitation the electronic transition energy levels are possible when this obey the rules for allowed transitions [11, 12].

For example for octahedral symmetry, the tetragonal distortion could provide a high Δ for d^3 electrons them could be arrangement in levels B_{2g} and E_g resulting spin $S = 1/2$, **Figure 6(A)**. For example for tetrahedral symmetry, the tetragonal distortion could provide a high Δ for d^3 electrons them could be arrangement in levels A_{1g} and B_{1g} resulting spin $S = 1/2$, **Figure 6(B)**.

For the tetragonal symmetry, the degeneracy of the E_g (d_{z^2} and $d_{x^2-y^2}$ orbitals) term is no affected by the spin orbit coupling and by Jahn-Teller theorem applies. The orbital degeneracy is lifted and the energy of the system lowered by a displacement of the ligands on the z-axis [11, 12]. An elongated or compressed of the coordination tetrahedron (or tetragonal distortion) leads to the energy level scheme shown in **Figure 6(B)** with unpaired electron in the $d_{x^2-y^2}$ orbital. The measure of EPR spectra is limited to the Zeeman splitting imposed by an external field on the unpaired electron in the non-degenerated $d_{x^2-y^2}$ orbital and one could think that the spin system can now be described by the spin Hamiltonian with $S = 1/2$ since the ground state is non-degenerate and has only associated spin angular momentum [9–15].

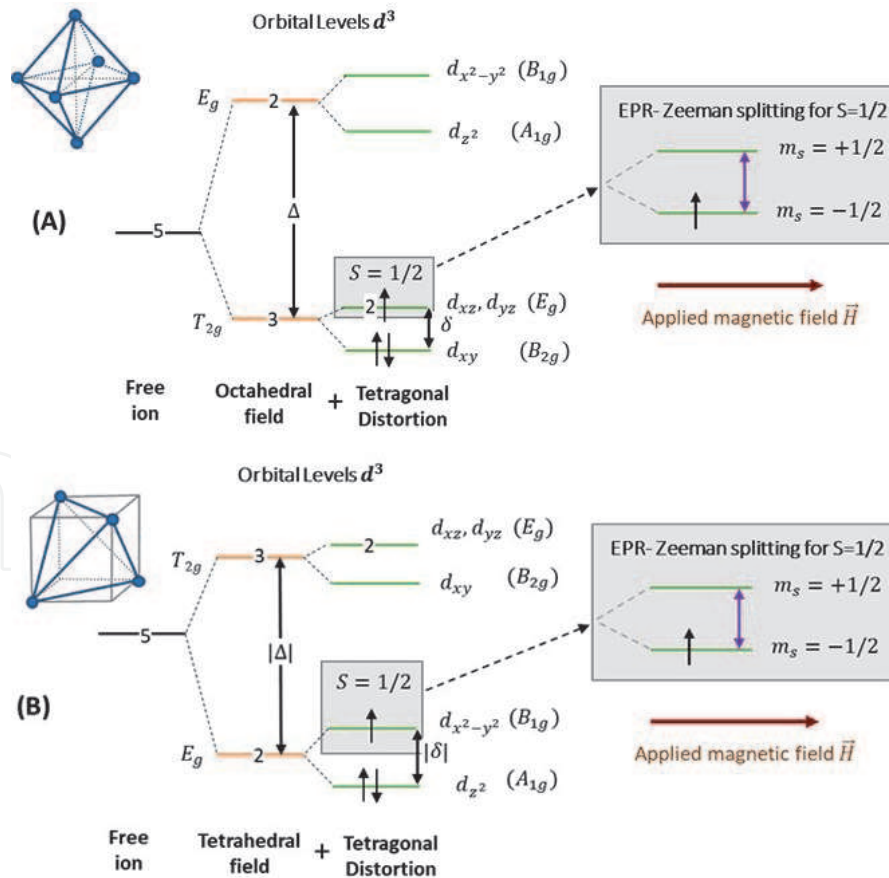


Figure 6.

Splittings and degeneracies of orbital levels d^1 or d^6 ions in two types of electric field caused by negative charges for (A) octahedral field ($\Delta > 0$) plus tetragonal distortion and (B) tetrahedral field ($\Delta < 0$) plus tetragonal distortion. For d^4 and d^9 ions applied to octahedral and tetrahedral fields. Shifting of the center of gravity of the set of levels is ignored [9–15]. If Δ is high, then the spin S is weak, and this yields low spin complexes and weakly paramagnetic. For example, for tetrahedral field, if Δ is high for d^3 electrons them could be arrangement in levels A_{1g} and B_{1g} yield a spin $S = 1/2$.

5. Characterization ceramic

The $Pb_{0.95}Sr_{0.05}(Zr_{0.53}Ti_{0.47})O_3 + x\%wtCr_2O_3$ is a ferroelectric ceramic powder, and it is possible to characterized by x-ray and electric measures [8, 16]. The EPR measures were taking at Biophysics and Magnetic Measure National Polytechnic Institute Laboratory using an EPR JEOL JES-RE3X spectrometer, **Figure 7**.

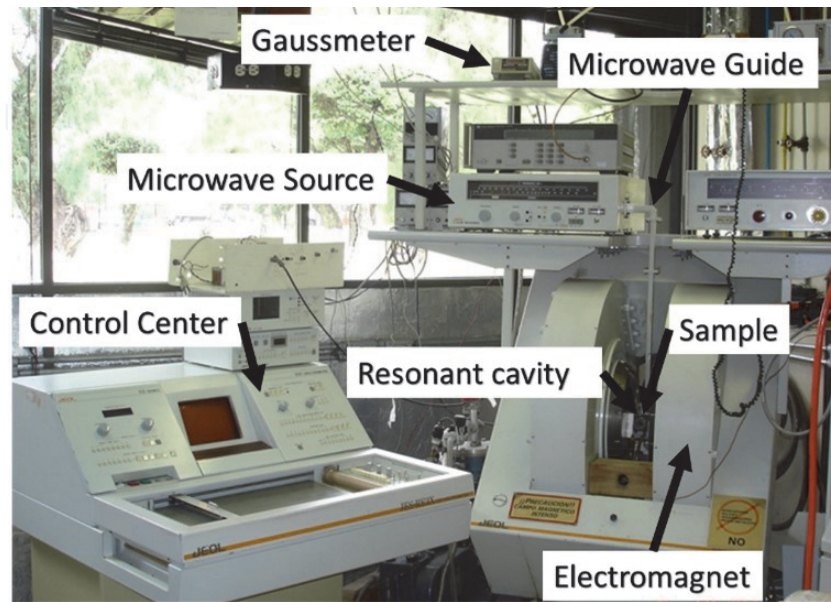


Figure 7.
EPR JEOL spectrometer [23].

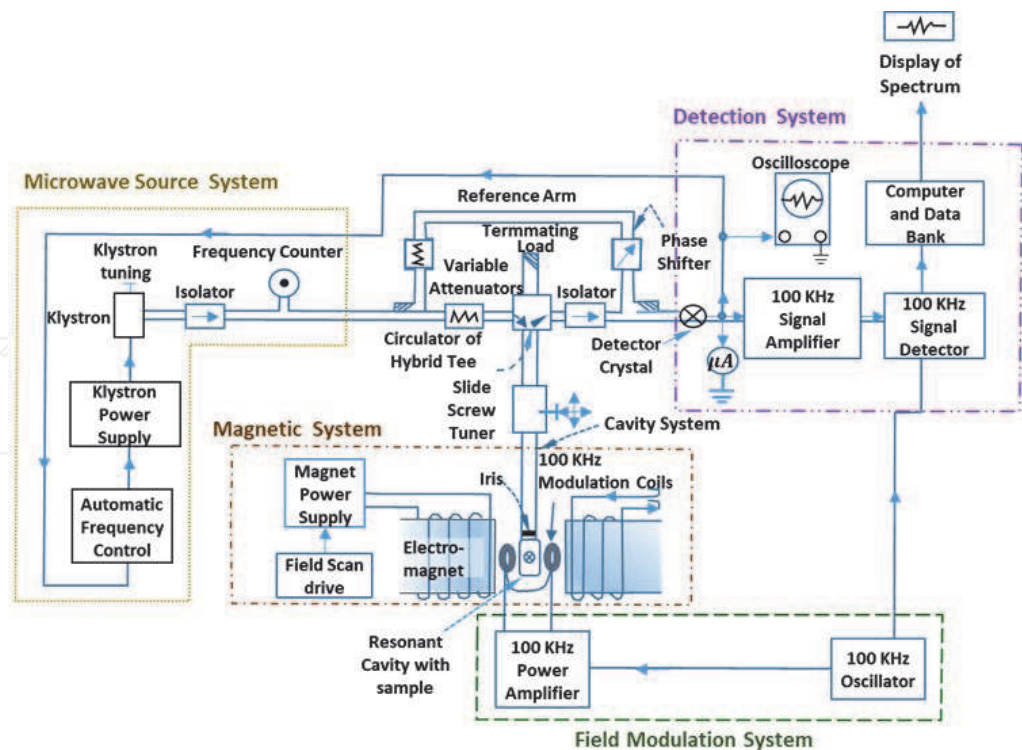


Figure 8.
General diagram for paramagnetic resonance spectrometer (EPR) that consist of magnetic system (electromagnet, modulation coils, magnet power supply and field scan drive), field modulation system (power amplifier, 100 kHz oscillator), cavity system (resonant cavity with sample, iris and the T-magic system), microwave source system (klystron power supply, automatic frequency control, etc.) and detection system (detector crystal, 100 kHz signal detector, 100 kHz signal amplifier, oscilloscope, computer and data bank; and display of the spectrum) [12].

The temperature measures were at 300K and 77K. The power potency was varied from 1 mW until 40 mW [17–23], at 9.45GHz microwave frequency at X-band. The lead zirconate titanate was doped with five percentages of Cr of 0%, 1%, 2%, 4% and 5%, we called the samples 0, 1, 2, 4 and 5 respectively.

The spectrometer is connected to workstation ES-PRIT to HP-9000 computer with a converter analogic digital target (A/D). The programing package performs acquisition, proccession and simulation data [23, 24]. The block diagram typical X-band EPR spectrometer employing 100KHz phase sensitive detection is shows in **Figure 8** [12, 23].

6. Results and discussions

The X-rays and electric measured was published by F. Calderon, and Yañez, et al. [8], the x-rays spectra are show in **Figure 9** for samples 4 and 5. The X-rays program fixed the $Pb(Zr_{0.44}Ti_{0.56})O_3$ compound and this do not detect secondary phases. The quantity of chromium is not enough for be detected by X-rays measures, because the limit detection is 5% of the element. About electric measured, when the chromium concentration varies from sample 1 to 5, the Curie's temperature value increases. The Cr substitution causes a tetragonal distortion field to the tetrahedral symmetry structure causes energy splitting effect by zero splitting field [12]. Due to the Cr^{3+} quantity is more than Ti^{4+} or Zr^{4+} quantities, the system tetragonality be modified and the grain size is increased [8]. The Curie's temperature varies slightly, and the energy activation is below and above to the transition.

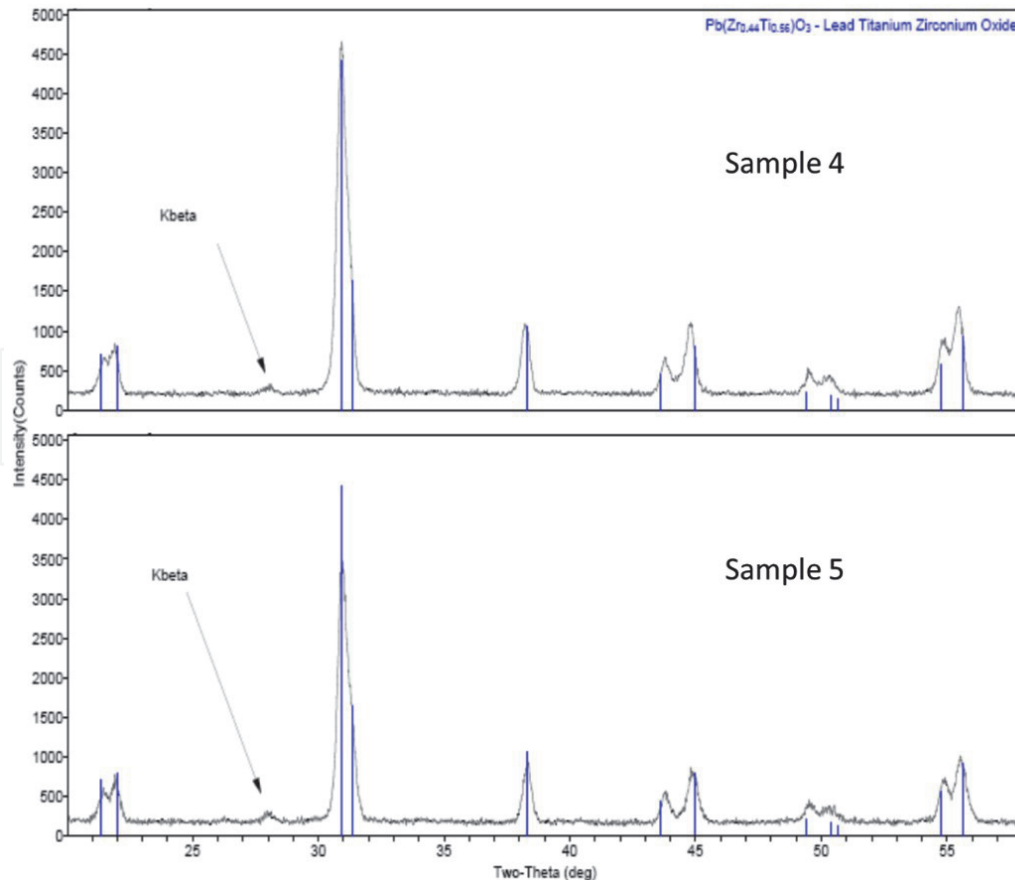


Figure 9.
X-rays for 4 and 5 samples that corresponds to perovskite structure or tetrahedral symmetry from $Pb(Zr_{0.44}Ti_{0.56})O_3$.

The presence of chromium determined by EPR guaranteed an oxygen or hold vacancy mechanism, also this effect was confirmed by Yañez, et al. [8].

6.1 EPR measured and results

The EPR spectrum were obtained for powder ferroelectric at 300 K. The EPR measures for the zero sample produce a spectrum with signals *R* and *C*, see **Figure 10**. The signal *R* had $g = 2.1295$ at 317 mT field. The signal *C* had several values $g_{\parallel} = 1.9194$, $g_{\perp} = 1.9355$ and $g_{iso} = 1.9301$. The intensity of signal *C* is low and this indicate that insipidus presence of the paramagnetic center. The signal corresponds to uniaxial local symmetry on the tetrahedral perovskite structure [12]. Even when the microwave power is increased there are no signals of saturation effects for all samples, this indicate that the paramagnetic center is stable and maintain their interaction neighbor stable.

The 1, 2 and 5 samples at 300 K and 77 K shows the same spectrum except the intensity increases from sample 2 to sample 5, the spectra for samples 2 and 5 are show in **Figures 11** and **12** respectively. For sample 1, the signal *B* had $g_{B\perp} = 1.9731$ and $g_{B\parallel} = 1.9441$; the signal *B** had $g_{B^*\perp} = 1.9352$ and $g_{B^*\parallel} = 1.9257$ spectroscopy parameters. For sample 2, there are two signals *B* and *B** too showed in **Figure 8**, for signal *B* was obtained $g_{B\perp} = 1.9720$ and $g_{B\parallel} = 1.9462$ at 345.20 mT and 350.31 mT respectively magnetic fields. For signal *B** $g_{B^*\perp} = 1.9360$ and $g_{B^*\parallel} = 1.9204$ at 352.14 mT and 355.00 mT respectively magnetic fields. When the Cr^{+3} substituted the Ti^{+4} ion, the tetragonality decreases [8].

The **Figure 13** shows the spectrum for sample 4 with the signals *B* and *B** too, but additionally shows the *G*, *H* and *DPPH* signals. For signal *B* the $g_{B\perp} = 1.9762$ and $g_{B\parallel} = 1.9424$ at 344.74 mT and 350.71 mT respectively. For signal *B** $g_{B^*\perp} = 1.9384$ and $g_{B^*\parallel} = 1.9189$ at 351.43 mT and 355.00 mT respectively. The *G* signal had $g_G = 2.0755$ at 328.21 mT . The signal *H* had $g_H = 2.1449$ at 317.6 mT field. The signal for *DPPH* had $g = 2.0036$ at 340 mT expected value for the EPR standard paramagnetic marker.

The analysis of EPR results start from chemical composition for ferroelectric $\text{Pb}_{0.95}\text{Sr}_{0.05}(\text{Zr}_{0.53}\text{Ti}_{0.47})\text{O}_3 + x\%wt\text{Cr}_2\text{O}_3$ from the spin electronic arrangements for

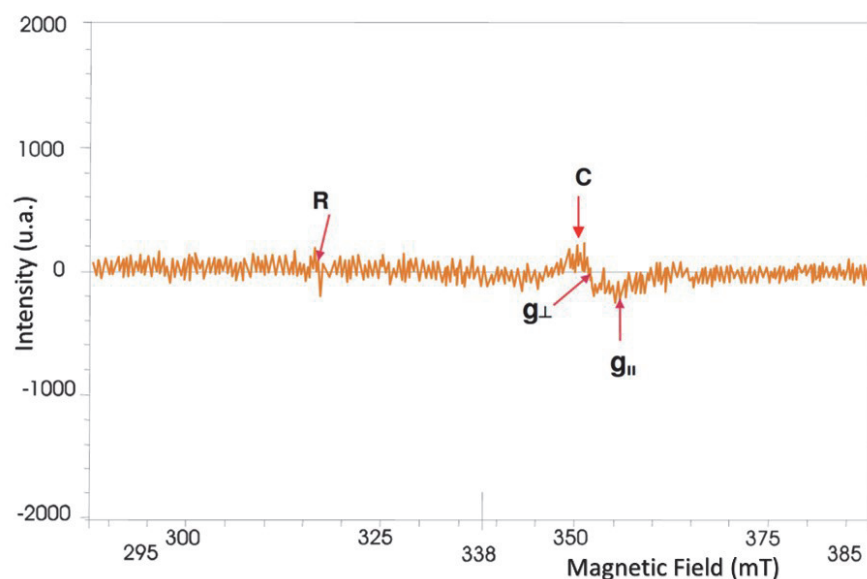


Figure 10.
 Zero sample spectrum shows *R* and *C* signals.

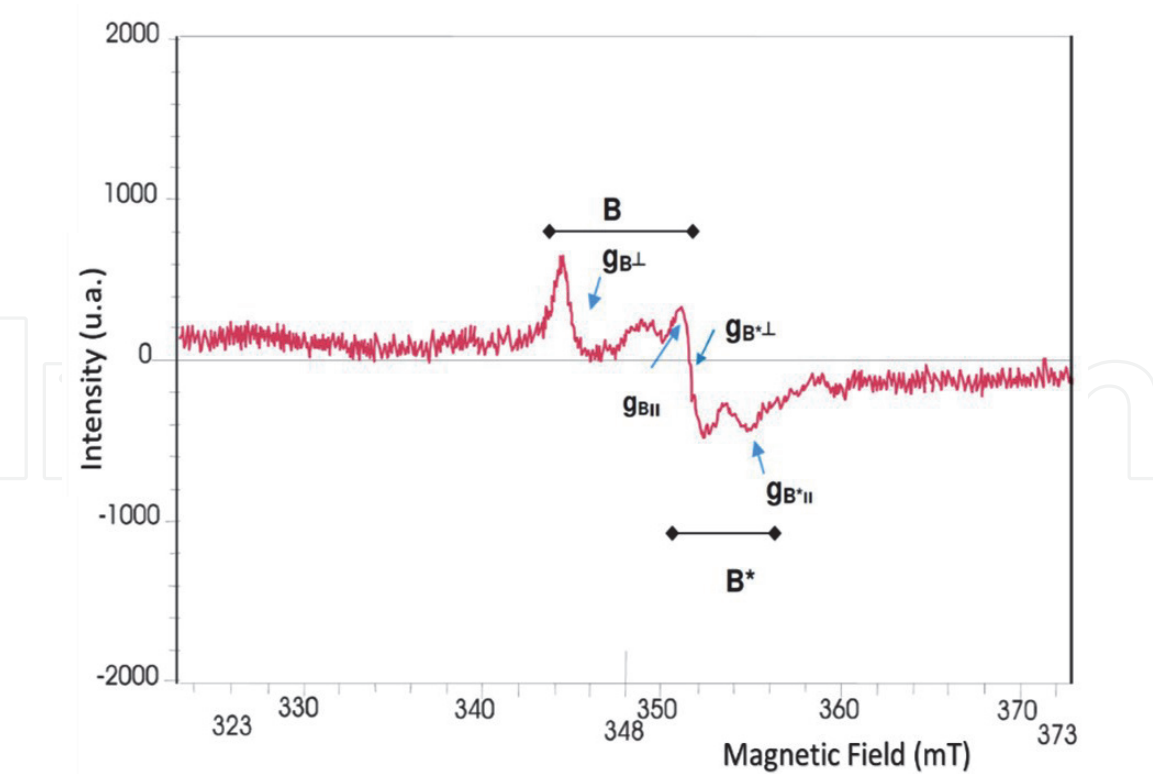


Figure 11.
EPR spectrum for sample 2. There are two signal groups B and B*.

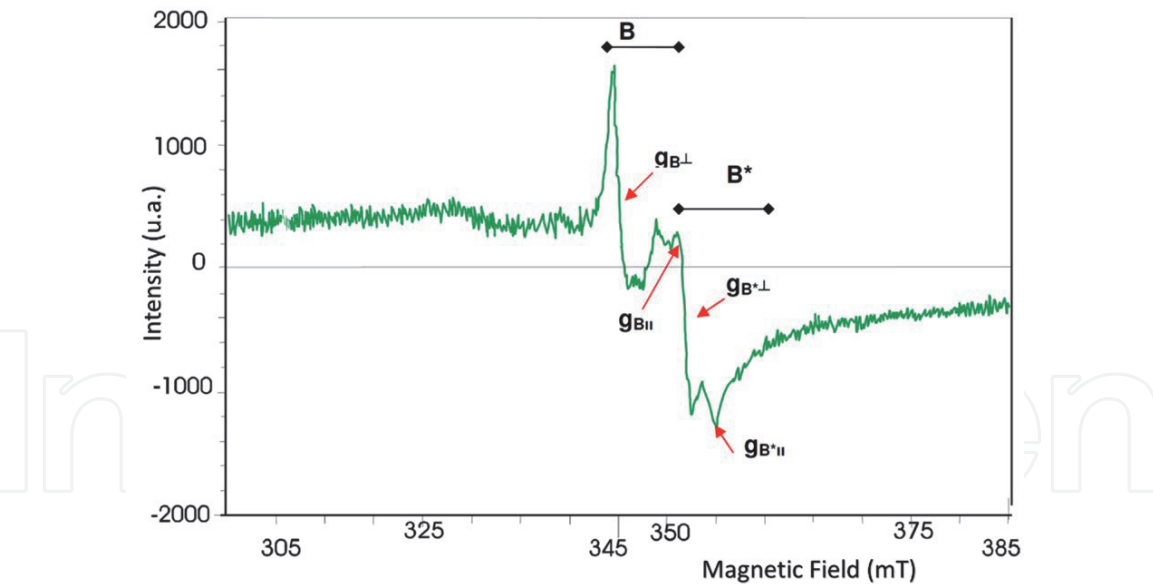


Figure 12.
EPR Spectrum for sample 5.

each element atom composition. The Cr had $1s^2 2s^2 2p^6 3s^2 3p^6 4s^2 3d^4$ electronic arrangement with +6, +5, +3 and +2 oxidation states. The chromium compounds with Cr^{+6} oxidation state are no paramagnetic, because the $1s^2 2s^2 2p^6 3s^2 3p^6 4s^0 3d^0$ electronic configuration had no unpaired electron. The Cr^{+5} had $1s^2 2s^2 2p^6 3s^2 3p^6 4s^0 3d^1$ electronic configuration with unpaired electron and 5/2, 3/2 and 1/2 spin state corresponding to low, medium and high spin respectively. For Cr^{+3} the spin states could be 1/2 and 3/2, corresponding to weak

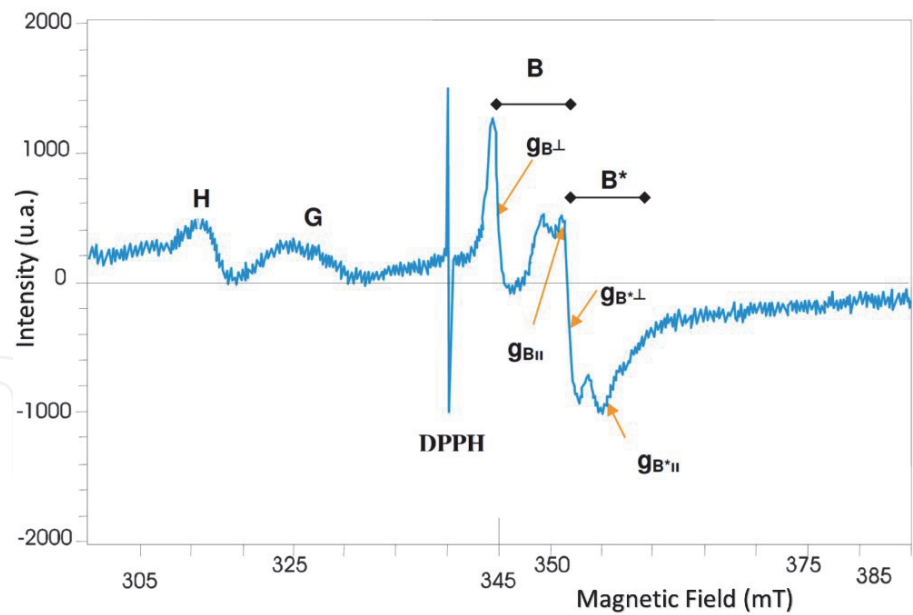


Figure 13.
EPR spectrum for sample 4.

and medium crystalline field split respectively. The Cr^{+2} is no paramagnetic by the $1s^2 2s^2 2p^6 3s^2 3p^6 4s^0 3d^4$ electronic configuration, i.e., had four paired electrons in d-orbital, this is because we have a octahedral crystalline structure into the perovskite structure that causes electronic levels split (Zero field splitting); this split have a high energy levels separation and the electrons unfollows Hund's rule, see **Figure 6(A)**, this causes that electrons stays at lowers energy levels, all this is because the experimental g-values are less than 2.00 for all spectrum, **Figure 10–13**. The other elements are not paramagnetic [19, 20, 24–26]. The titanium has 4+ the state oxidation (Ti^{4+}), and the lead state oxidation is +2 (Pb^{2+}), both elements have not uncoupled electrons and they cannot be detected by EPR. Only Cr^{3+} or Cr^{5+} signals are expected in the EPR spectrum.

From chemical composition $Pb_{0.95}Sr_{0.05}(Zr_{0.53}Ti_{0.47})O_3 + x\%wtCr_2O_3$ with $x = 0.0, 0.1, 0.2, 0.4$ and 0.5 , to sites B the Zr^{4+} is substitute for Ti^{4+} and to sites A the Sr^{2+} is substitute for Pb^{2+} in perovskite structure of the material [1–4, 25–27]. Additionally, in **Figure 14** shows how Cr is introduced to substitute Ti in sites B for the samples [8, 25–27]. The sample zero no contained Cr and it was taken like the control sample or EPR blank sample.

The **Figure 15** shows the EPR spectrum for sample 0 at 300 K. The R signal is at 317 mT and $g = 2.0134$. The C signal is axial $g_{\perp} = 1.965$ and $g_{\parallel} = 1.9181$; bout signals are small at noise level. Thus, the blank sample, whose chemical formula indicates that it should not give an EPR spectrum, shows the R resonance, which is

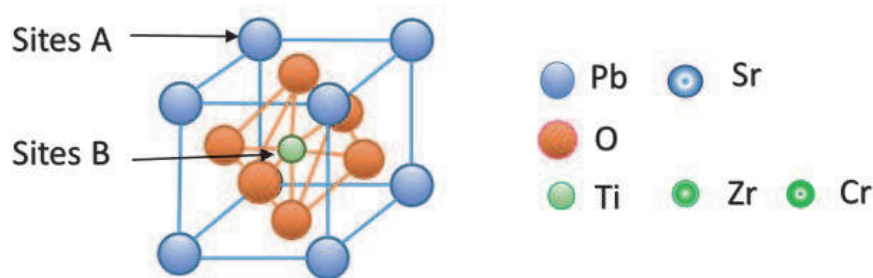


Figure 14.
Perovskite structure for ferroelectric $Pb_{0.95}Sr_{0.05}(Zr_{0.53}Ti_{0.47})O_3 + x\%wtCr_2O_3$ with $x = 0.0, 0.1, 0.2, 0.4$ and 0.5 .

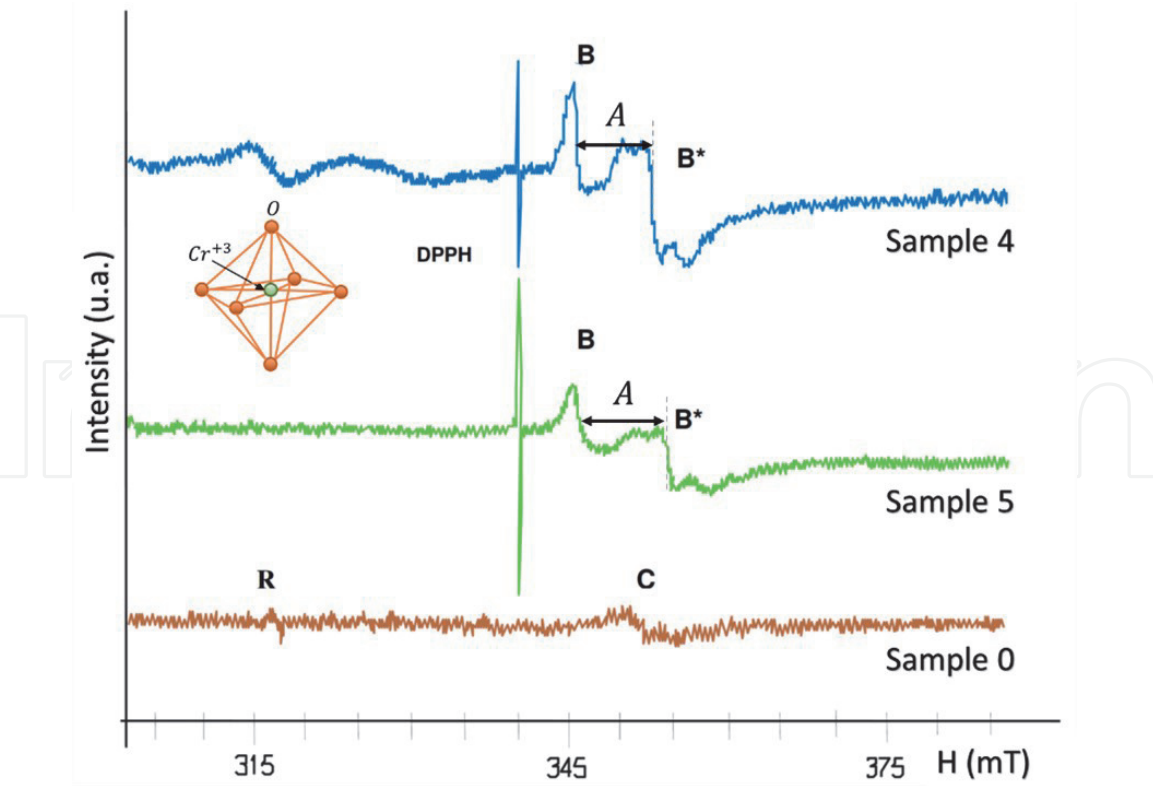


Figure 15. EPR spectra for 1, 5 and 4 samples at 300 K. the two B and B* oblate axial signals are typical by powder samples with $g_{\perp} > g_{\parallel}$ and hyperfine interaction $a_o = A$.

due to Fe^{3+} , and the C axial signal corresponds to Cr spectrum. When the temperature is low to 77 K, the R signal disappears and the C signal decreases. The Cr in this sample comes as manufacturing impurity. The 1, 2 and 5 samples show at 300 K and 77 K the same line shape spectrum, and the intensity increase from 1 to 2 and to 5. The increased intensity is due to percentage increase of Cr from 1% to 2% and 5% because the area under curve absorption EPR is proportional to the number of paramagnetic ions [9–12]. The typical EPR spectrum for the samples 0, 4 and 5 with g values less to 2.00 were obtained, see **Figure 15**. The DPPH signal is at left to the spectrum this means that Cr paramagnetic ions are d^3 with low spin $1/2$ of Cr^{3+} [9–18]. This case is analogous for Mn^{4+} , $S = 1/2$ in the ferroelectric $Pb(Ti,Mn)O_3$ [27] that is isoelectronic with Cr^{3+} . The low spin value of $S = 1/2$ is caused by the tetragonal distortion in the octahedral symmetry (Cr-O) that increase the crystal field factor Δ , like is shows in **Figure 6(A)** [9–12]. These results are compatibles with the photoluminescence results found by Yanez et. al. for the same compound [8].

The four features of the spectrum are explained with two B and B* oblate axial signals typical by powder with $g_{\perp} > g_{\parallel}$ and hyperfine interaction $a_o = A$. The parameters are summarized in **Tables 1** and 2, corresponds to a system with $S = 1/2$.

Sample	B Signal			
	g_{\perp}	g_{\parallel}	g_{iso}	A (mT)
0	—	—	—	—
1	1.9731	1.9441	1.9634	4.93
2	1.9720	1.9462	1.9634	4.75
5	1.9726	1.9424	1.9625	5.89

Sample	B Signal			
	g_{\perp}	g_{\parallel}	g_{iso}	A (mT)
4 (300 K)	1.9762	1.9424	1.9649	5.89
4 (77 K)	1.9733	1.9448	1.9651	5.73

Table 1.
EPR parameters for B signal.

Sample	B^* Signal			
	g_{\perp}	g_{\parallel}	g_{iso}	A (mT)
0	1.9355	1.9194	1.9301	3.26
1	1.9352	1.9257	1.9310	2.97
2	1.9360	1.9204	1.9308	2.86
5	1.9350	1.9189	1.9296	3.10
4 (300 K)	1.9384	1.9189	1.9319	3.57
4 (77 K)	1.9372	1.9181	1.9308	3.33

Table 2.
EPR parameters for B^* signal.

For each B and B^* signal corresponds one Cr^{3+} , with spin $S = 1/2$, which is substituting to Ti^{4+} or Zr^{4+} in B sites into the octahedral symmetry with tetragonal distortion (high symmetry) slightly different one to other [27]. One of these cells correspond to octahedron with Cr^{3+} belong to crystalline cells localized into the ferroelectric grains, and the other belongs to crystalline cells on surface of the material grains. This interpretation is consistent with the interpretation published of the B and B^* sites distinguished of Mn^{4+} in $PbTiO_3$ [27].

6.2 Microwave power variation

The microwave power was varied from 1mW to 40mW for the samples and there is no change for EPR spectrum. The intensity of all features of the spectrum increase due power increase without differentiation. No distortion of the line shape of spectra is detected either, so until 40 mW power there is no sample saturation [9–18]. Qualitatively the 1, 2 and 5 samples present the same spectrum, but the quantitatively the EPR parameters change, **Tables 1** and **2**.

In addition to signals B and B^* the spectrum of sample 4 shows the isotropic G and H signals located at $g_H = 2.1449$ and $g_G = 2.0755$ respectively. By having these signals g values greater than 2.00 but around to zone to $g = 2.00$ and because they are anisotropic could be identified like two of three expected fine lines for Cr^{3+} , $s = 3/2$, it present the Zeeman split in a little crystalline field [5, 10, 14]. The positive deviation sign of value 2.0036 is explained for considerable difference between excited energy levels in ground state by Lx , Ly and Lz operators [12–18].

The signals B and B^* in the EPR spectrum for sample 4 at 77 K no changes respect to spectrum at 300 K, **Tables 1** and **2** but in the region for G and H signal at 77 K a third isotropic line with $g = 2.0716$ is resolved. The power variation study no shows changes line shape or line number or saturation effects at 300 K from 1 to 40 mW for this sample.

7. Conclusions

The ferroelectric $Pb_{0.95}Sr_{0.05}(Zr_{0.53}Ti_{0.47})O_3 + x\%wtCr_2O_3$ with $x = 0.0, 0.1, 0.2, 0.4$ and 0.5 samples produce a characterized spectrum well defined by absorption peaks. The signals B and B^* are present in the EPR spectrum for all samples doped with Cr and they no have saturation features for microwave power variation from 1 mW to 40 mW at $300K$ and $77K$. Both B and B^* signals correspond to Cr^{3+} ion, with spin $S = 1/2$ which is substituting to Ti^{4+} or/and Zr^{4+} ions at B sites. One of signals corresponds to octahedron with Cr^{3+} ions belong to crystalline cells with tetragonal distortion localize into the grains. The other signal corresponds to octahedrons crystalline cells localize cells in the frontiers between the material grains, i.e., the EPR spectra shows two distinguishable B sites, which have been registered by B and B^* signals. The two B sites are similarly to B and B^* sites of Mn^{4+} in $PbTiO_3$ reporter in reference [27]. The microwave power increase does not increase the signals intensity separately, this means that the spectrum is not a superposition of two or more signals corresponding to different paramagnetic centers. The line width and the g -values are not changing with temperature or microwave power variation. The sample 4 shows the same spectrum for 0, 1, 2 and 5 samples. However, the sample 4 shows additionally the H and G signals forming a “fine triple” structure which indicates the Cr^{3+} presence at weak crystalline field environment in to local octahedral symmetry.


Author details

Veronica Lucero Villegas Rueda

Basic Sciences Department, Professional Interdisciplinary Unit of Engineering and Advanced Technology - IPN, Mexico City, Mexico

*Address all correspondence to: veyarle@gmail.com

IntechOpen

© 2021 The Author(s). Licensee IntechOpen. This chapter is distributed under the terms of the Creative Commons Attribution License (<http://creativecommons.org/licenses/by/3.0>), which permits unrestricted use, distribution, and reproduction in any medium, provided the original work is properly cited. 

References

- [1] Scott J. F., Applications of Modern Ferroelectrics. *Science*.2007; 5: 954–959. DOI: 10.1126/science.1129564
- [2] Irzaman H., Ferroelectrics and Their Applications. IntechOpen, 2018. DOI: 10.5772/intechopen.73075
- [3] Blázquez A., García A and Carrascosa M. Biological applications of ferroelectric materials. *Applied Physics Reviews* 2018; 5: 041101; DOI:10.1063/1.5044472
- [4] Kim T. Y., Kim S. K. and Kim S. W., Application of ferroelectric materials for improving output power of energy harvesters. *Nano Convergence* 2018 Dec; 5: 30. DOI: 10.1186/s40580-018-0163-0
- [5] Calderón P. F., Oscilaciones Electromecánicas y pérdidas en cerámicasferroeléctricas [Thesis]. La Habana Cuba. Facultad de Física-IMRE, Habana University; 1999.
- [6] Ramírez R. D., Estudio EPR de la reducción del Mn^{4+} a Mn^{2+} en el $PbTiO_3$ Modificado [Thesis]. Ciudad de México, ESFM-National Polytechnic Institute; 2004.
- [7] Wersing W., Libitz K. and Mahaupt J., Anisotropic Piezoelectric effect in modified $PbTiO_3$ ceramics, *IEEE Transactions on Ultrasonics ferroelectrics and frequency control*; 36 (4):424–433, 1989.
- [8] Hernández M., Durruty D., Costa J., Calderón F., Guerra J. and Yañez J. M., Photoluminescence in $Pb_{0.95}Sr_{0.05}(Zr_{1-x}Ti_x)_{1-y}Cr_yO_3$ ferroelectric ceramic system. *Journal of Applied Physics* 2014; 116: 043510. DOI:10.1063/1.4885762
- [9] Drago R. S. Physical Methods for Chemistry. 2nd Ed. Surfside Scientific Publishers 1992. 660 p.
- [10] Burns R. Mineralogical Applications of Crystal Field Theory, Cambridge Topics in Mineral Physics and Chemistry. Cambridge University Press 1964. 480 p.
- [11] Roessler M. and Salvadori E. Principles and applications of EPR spectroscopy in the chemical sciences. *Chemistry Society Review*, 2018; 47: 2534. DOI: 10.1039/c6cs00565a
- [12] Weil J. and Bolton J. Electron Paramagnetic Resonance: Elementary theory and practical application. Wiley, New Jersey 2007. 687 p.
- [13] Zamorano R., El uso de EPR en la caracterización de compuestos con metales de transición, Academia Mexicana de Química Inorgánica, A.C. y CINVESTAV-IPN, México 4–21, 1993.
- [14] Gordy W. Theory and Applications of Electron Spin Resonance, Duke University, John Wile & Sons 1980.
- [15] Carrington A. and McLachlan A. D., Introduction to Magnetic Resonance, Harper and Row, New York 1979.
- [16] Pilbrow M. Transition Ion Electron Paramagnetic Resonance, Clarendon Press, Oxford, 1990.
- [17] Feher G. Electron Paramagnetic Resonance with Applications to Selected Problems in Biology, Gordon and Breach Science Publishers 1969.
- [18] Zadrozny J. M., Greer S. M., Hill S. and Freedman D., A flexible iron(II) complex in which zero-field splitting is resistant to structural variation. *Chemical Science* 2015. DOI: 10.1039/c5sc02477c
- [19] Álvarez G., Caracterización de la absorción de potencias en materiales ferroeléctricos a muy altas frecuencias

[Thesis], ESFM-National Polytechnic Institute., México DF. 2006.

[20] Ramírez D. y Zamorano Ulloa R., Obtención Experimental de Señales en Resonancia Paramagnética Electrónica, Reporte Interno ESFM/F08/93, ESFM-National Polytechnic Institute, México 1993.

[21] Ramírez D., Resonancia de Espín Electrónica del compuesto (Mn(Pidieno (H₂O)₂)Cl 4H₂O [Thesis]. ESFM-National Polytechnic Institute, México 1994.

[22] Jeol, Instructions ESR Spectrometer, Ed. Jeol LTD, Tokio, Japan, 1992.

[23] Basurto E. y Zamorano R., Simulación de espectros en el Software ESPRIT, Reporte Interno ESFM/F06/93, ESFM- National Polytechnic Institute, México 1993.

[24] Keeble D.J., Poindexter E. H. and Gerardo G.J., Electron Paramagnetic Resonance Studies of impurity defects in PbTiO₃, Appl. Spectroscopy, 51(1); 1997:117–122

[25] Lian Xing He, et al, Effects of Cr₂O₃ addition on the piezoelectric properties and microstructure of PbZr_xTi_y(Mg_{1/3}Nb_{2/3})_{1-x-y}O₃ ceramics J. of European Ceramic Society 2001:703–709. DOI:10.1016/S0955-2219(00)00256-9

[26] Mabbs F.E. and Collins D., Electron Paramagnetic Resonance of d Transition Metal Compounds, Elsevier, Amsterdam, 1992.

[27] Ramírez Rosales D., Zamorano Ulloa R., Electron spin study of the conversion of Mn⁴⁺ to Mn²⁺ in the Pb_{1-x}Eu_xTi_{1-y}Mn_yO₃ ceramic system, Solid Stated Commun. 118; 2001: 371–376. DOI: 10.1016/S0038-1098(01)00072-2